High Pressure–High Temperature Decomposition of γ-Cyclotrimethylene Trinitramine

ARTICLE *in* THE JOURNAL OF PHYSICAL CHEMISTRY A · SEPTEMBER 2012

Impact Factor: 2.69 · DOI: 10.1021/jp307373v · Source: PubMed

3 AUTHORS, INCLUDING:

Zbigniew Dreger
Washington State University
122 PUBLICATIONS **1,121** CITATIONS
SEE PROFILE

Matthew D Mccluskey
Washington State University
139 PUBLICATIONS **2,378** CITATIONS
SEE PROFILE

THE JOURNAL OF PHYSICAL CHEMISTRY A

Article

pubs.acs.org/JPCA

High Pressure–High Temperature Decomposition of γ-Cyclotrimethylene Trinitramine

Zbigniew A. Dreger,* Matthew D. McCluskey, and Yogendra M. Gupta

Institute for Shock Physics and Department of Physics, Washington State University, Pullman, Washington 99164-2816, United States

ABSTRACT: Decomposition of γ-cyclotrimethylene trinitramine (γ-RDX) under high pressure–high temperature conditions was examined to elucidate the reactive behavior of RDX crystals. Vibrational spectroscopy measurements were obtained for single crystals in a diamond anvil cell (DAC) at pressures from 6 to 12 GPa and temperatures up to 600 K. Global decomposition rates, activation energies, and activation volumes at several pressures and temperatures below the $P-T$ locus for the γ-RDX decomposition were obtained. Similar to ε-RDX, but in contrast to α-RDX, we found that pressure decelerates the decomposition of γ-RDX. The decomposition deceleration with pressure in the γ-phase can be attributed to pressure-inhibiting bond homolysis step(s). The main decomposition species were identified as N_2O, CO_2, and H_2O, in accord with the species reported for the α-phase decomposition at high pressures. This work complements previous studies on RDX at HP–HT conditions and provides comprehensive results on the reactive behavior of γ-RDX; the γ-phase plays a key role in RDX decomposition at $P-T$ conditions relevant to shock wave initiation.

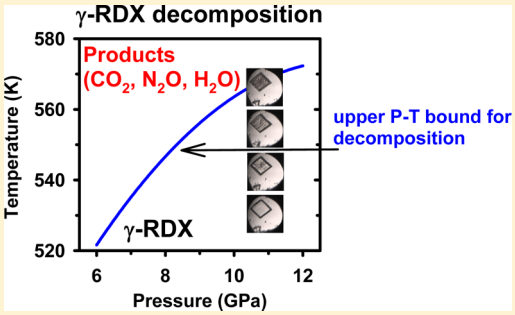

1. INTRODUCTION

A good understanding of the response of high explosives (HE) at high pressures and high temperatures is important for addressing performance and safety issues. In particular, detailed knowledge of structural and chemical stabilities is necessary to understand the reactive behavior of HE crystals over the range of pressures and temperatures relevant to shock wave initiation.

Here, we report on the chemical decomposition of single crystals of cyclotrimethylene trinitramine (RDX; $(CH_2NNO_2)_3$) at high pressures and high temperatures (HP–HT). RDX is one of the most important energetic crystals, and it is widely used in explosives and monopropellants. Extensive spectroscopic and X-ray diffraction studies have shown that, depending on the external conditions, RDX can exist in several polymorphic phases: α, β, γ, δ, and ε.[1−13] Three of these phases (α, γ, and ε) can exist at HP–HT conditions and can, therefore, contribute to decomposition. Furthermore, early reports conjectured that the ε-phase (incorrectly identified as β-phase initially)[2,3] can play an important role in shock-induced decomposition. Thus, the study of the structural and chemical stability of this phase has attracted attention.[2,3,11−13] It was established that ε-RDX has limited stability at high pressures and high temperatures, and decomposes readily according to an autocatalytic rate law.[11] Importantly, this phase was found to be formed only in a narrow pressure domain.[11,12]

The combination of shock wave experiments[14,15] and recent static high pressure work[16] has demonstrated that the γ-phase of RDX, not ε- or α-phase, is involved in shock-induced decomposition. Therefore, a good understanding of the γ-RDX response at HP–HT conditions is important for elucidating the reactive behavior and decomposition mechanisms of RDX at the conditions relevant for shock initiation. Unlike the other two HP–HT phases of RDX, the decomposition of the γ-phase has not been studied, except in our preliminary work reported recently.[16] In that work, we provided evidence that γ-RDX, in contrast to previous reports,[3] decomposes at HP–HT conditions without involvement of other phases. Here, we have focused on the γ-phase decomposition kinetics at various pressures and temperatures below the $P-T$ upper bound for decomposition. The specific objectives of this work were (1) to determine pressure effects on decomposition kinetics, (2) to identify decomposition products, (3) to gain insight into the decomposition mechanism, and (4) to relate the γ-phase decomposition results to those for the other two HP–HT phases of RDX. These data are expected to be valuable for future computational studies on RDX decomposition at HP–HT conditions. As in earlier work,[11,12,16] we use HP–HT vibrational spectroscopy measurements on single crystals to monitor the decomposition.

The remainder of this paper is organized as follows. Experimental procedures are described briefly in section 2. Sections 3 and 4 present the experimental data and discussion regarding the γ-RDX decomposition kinetics, activation energies, and activation volumes, decomposition products, and mechanisms. The main findings of this work are summarized in section 5.

Received: July 25, 2012
Revised: September 7, 2012
Published: September 12, 2012

2. EXPERIMENTAL METHODS

The experimental approach was similar to that reported in our previous work.[11,12,16] Therefore, we mention only the key elements here. RDX single crystals were grown from an acetone solution using RDX polycrystals provided by Dr. D. E. Hooks of Los Alamos National Laboratory. The crystals were carefully selected to ensure similar size and quality. High pressures were produced in the samples using a diamond anvil cell (DAC). Spring-steel gaskets, pre-indented to 0.06−0.08 mm with a 0.125 or 0.200 mm hole drilled in the indentation, were used as sample compartments. A single crystal of RDX and a ruby chip were loaded into the sample compartment, and cryogenically loaded argon was used as an inert pressure transmitting medium. The ruby fluorescence method utilizing R-line shifts was used to monitor pressure. The precision of our pressure measurements at room temperature was estimated to be 0.05 GPa. The temperature of the DAC was varied by using a resistive heater wrapped around the cell. The sample temperature was monitored using iron−constantan thermocouples. The accuracy of the temperature measurements in our experiments was estimated to be ±2 K.

A micro-Raman system (T64000, JY-Horiba) equipped with a microscope (Olympus BX-40) was used to provide the spectra and images of γ-RDX at various pressures and temperatures. The 532 nm line from a CW diode-pumped solid-state (DPSS) laser (Verdi-Coherent) was employed for Raman excitation. To avoid any irreversible effects in the sample, the exposure time and the laser irradiation power were kept at a low level. Specifically, the incident power on the sample did not exceed 50 mW and the accumulation time of the Raman spectra was usually 2 s. Furthermore, the laser spot size was adjusted to acquire a signal from most of the sample, and was typically about 50 μm in diameter.

Raman experiments were carried out at pressures ranging from 6 to 12 GPa, and at temperatures ranging from ∼295 to 600 K. Measurements were carried out at constant temperatures to determine the decomposition rates at selected pressures and temperatures. In these experiments, the sample was heated at a rate of 2−3 K/min to the targeted temperature. This temperature was then maintained within ±1 K, and the Raman spectra were measured at 1 min intervals. The pressure was monitored and adjusted, in situ, as needed to maintain a constant pressure during the duration of each experiment.

The decomposition products from the samples quenched to room temperature were examined using a Fourier-transform infrared (FTIR) spectrometer (Bomem DA8), equipped with a liquid nitrogen cooled mercury cadmium telluride (MCT) detector.[17] The instrumental resolution was about 4 cm^{-1}, and the spectra were averaged over 10 000 scans. The FTIR spectra were corrected for absorption of the empty DAC, with the same gasket.

3. RESULTS

In our previous work, we determined the phase diagram of RDX crystal up to 12 GPa.[16] In Figure 1a we present a simplified version of this diagram to indicate the location of the γ-phase with respect to other phases. The close-up of the $P-T$ domain of the γ-phase is shown in Figure 1b. Raman measurements were obtained at the selected pressures and temperatures indicated in Figure 1b. These pressures and temperatures were located below the curve that determines the upper $P-T$ bound for the γ-phase decomposition. This curve

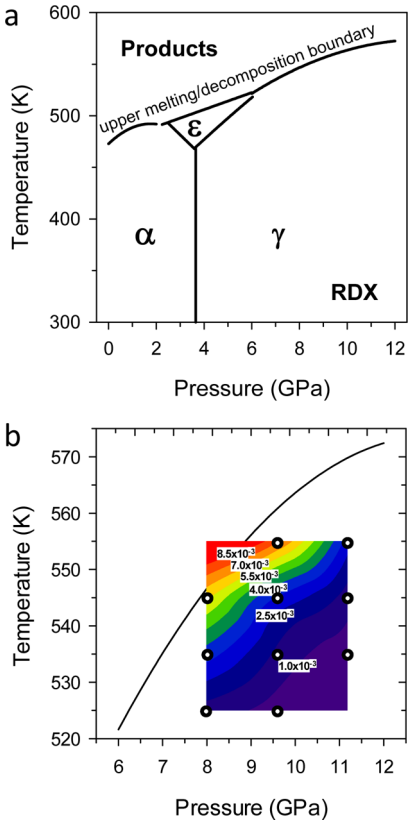

Figure 1. (a) Simplified version of the phase diagram of RDX,[16] where α, γ, and ε denote different RDX phases. (b) $P-T$ upper bound for the γ-phase decomposition (solid line). Decomposition kinetics were measured at pressures and temperatures indicated by circles. Contour graph, obtained with the SigmaPlot software, represents the resulting decomposition rates (see Table 1). Decomposition rates are given in s^{-1}.

demarcates two states of γ-RDX: the decomposed form, above the curve; the limited stability form, below the curve. In other words, as the γ-RDX approaches the $P-T$ conditions defined by the curve in Figure 1b, it becomes more chemically unstable and ultimately decomposes. Therefore, measurements at different $P-T$ values can provide insight into the mechanisms governing γ-RDX decomposition. Accordingly, an examination of decomposition kinetics is the first step in understanding these mechanisms.

3.1. Global Kinetics for Decomposition. To determine the decomposition kinetics, we monitored changes in the intensity of the Raman bands. Under unchanged experimental conditions (excitation intensity, and excitation and collection geometry), Raman intensity can be related to the number/concentration of molecules of interest. In other words, a decrease in the intensity of the Raman bands is indicative of a decreasing number of molecules, associated with the particular bands in the sample examined, and can, therefore, provide a measure of the extent of decomposition. In Figures 2 and 3, we show Raman spectra in the range from 750 to 1000 cm^{-1} and the corresponding optical images of γ-RDX, respectively, obtained at 8 GPa and 525 K, and at different times. Changes in the spectra and the images demonstrate the decomposition progress. As seen in the images in Figure 3, decomposition apparently originates at the local imperfections occurring at the sample surface due to the $\alpha-\gamma$ phase transition at 4 GPa. This observation demonstrates that the onset of decomposition can

dx.doi.org/10.1021/jp307373v | J. Phys. Chem. A 2012, 116, 9680−9688

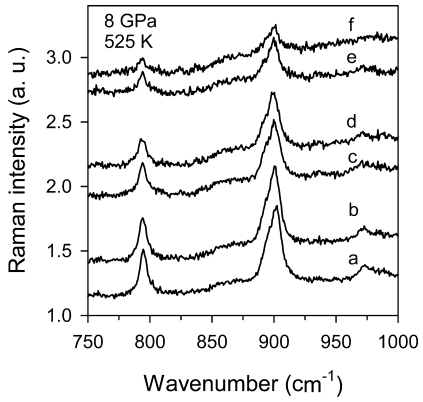

Figure 2. Selected Raman spectra of γ-RDX for CH_2 rocking + CN stretching (901 cm^{-1}) and C−N stretching and ring CNC stretching + NO_2 scissors (794 cm^{-1}) vibrations at 8 GPa and at different times after reaching temperature of 525 K: (a) 0 s; (b) 6.37×10^3 s (~1.77 h); (c) 8.67×10^3 s (~2.41 h); (d) 8.94×10^3 s (~2.48 h); (e) 9.55×10^3 s (~2.65 h); (f) 9.75×10^3 s (~2.71 h). Raman spectra were acquired for 2 s. The offset between the spectra results from an increase in the background light due to decomposition.

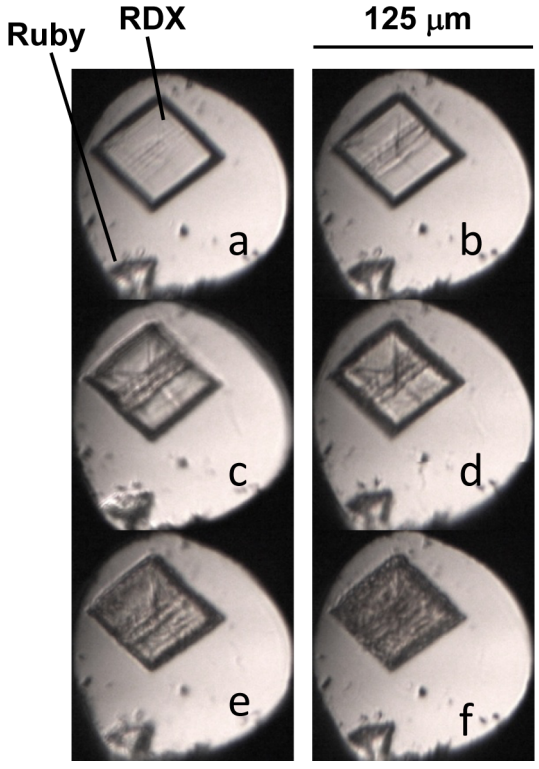

Figure 3. Images of γ-RDX crystal at 8 GPa and 525 K. Images correspond to the spectra shown in Figure 2. The hole diameter in the gasket was ~125 μm.

be affected by the presence of macroscopic defects. Therefore, care was taken to conduct experiments on crystals without noticeable imperfections.

To acquire information on Raman intensity changes as the decomposition proceeds, we followed changes in the intensity of several bands from 400 to 1300 cm^{-1}. The combined intensities from these bands were averaged and then normalized to one at $t = 0$ (starting time). For decomposition at a later time, the intensity was normalized with respect to the value at $t = 0$. The experiments were performed at several pressures and temperatures as indicated by the small circles in Figure 1b. Typical results of Raman intensity changes as a function of time, obtained at a selected temperature and different pressures and at a selected pressure and different temperatures, are shown in Figures 4a and 5a, respectively. In

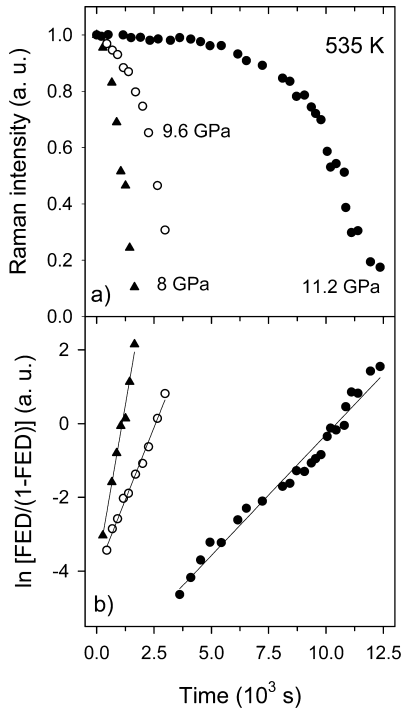

Figure 4. (a) Normalized intensity of selected Raman modes of γ-RDX as a function of time. Further descriptions can be found in the text. Data represent experiments at 535 K and at three different pressures. (b) Plots of fractional extent of decomposition (FED) as a function of time for data shown in panel a. Solid lines are from the least-squares fits to the experimental data. The global decomposition rates obtained from the fits are presented in Table 1.

general, these curves reveal similar features: an initial plateau, followed by an increasing slope, and finally, at the end, a decreasing slope. In the initial stages, referred to as the plateau or induction period, the rate of reaction is relatively slow. This is followed by another period of time, referred to as the accelerating period, in which the rate of reaction increases. Finally, this is followed by the third period, in which the rate of reaction decreases with time. The relative contributions of each these features depend on the pressure−temperature values in the experiment.

Because the Raman intensity decrease can be related to the extent of decomposition, we can obtain the fractional extent of decomposition (FED) by subtracting the values in Figures 4a and 5a from unity. FED plots as a function of time are commonly used in determining the kinetics of thermal reactions, including the decomposition of solids.[18] As shown in Figures 4b and 5b, our FED−time data can be fit to a relatively simple form of the autocatalytic rate equation:

$$\ln[\mathrm{FED}/(1 - \mathrm{FED})] = kt + C \quad (1)$$

where k is a global decomposition rate and C is a constant. Equation 1 is often identified with the Prout−Tompkins model,[18,19] describing the global kinetics of nucleation and growth as opposed to specific reactions. While it oversimplifies a complex process governing solid state decomposition, it

dx.doi.org/10.1021/jp307373v | J. Phys. Chem. A 2012, 116, 9680−9688

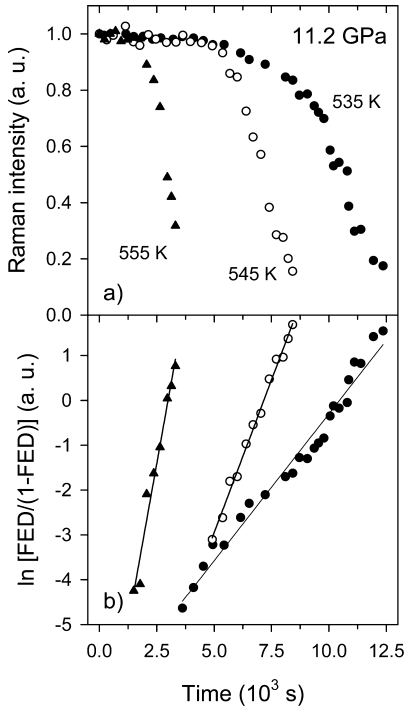

Figure 5. (a) Normalized intensity of selected Raman modes of γ-RDX as a function of time. Data represent experiments at 11.2 GPa and at three different temperatures. (b) Plots of fractional extent of decomposition (FED) as a function of time for data shown in panel a. Solid lines are from the least-squares fits to the experimental data. The global decomposition rates obtained from the fits are presented in Table 1.

permits a consistent extraction of the decomposition rates, even though the physical meaning of the rate is unclear.[11,18] It was used effectively in our previous work on the decomposition of ε-RDX,[11] and in work on other high explosives.[20]

The application of eq 1 to our data provides good fits (see Figures 4b and 5b) and can be used to evaluate the global decomposition rates for γ-RDX at various pressures and temperatures. The combined results are presented in Table 1 and in Figure 1 as a contour plot. They clearly demonstrate the deceleration of global decomposition rates with increasing pressure.

Table 1. Global Decomposition Rates of γ-RDX at Several Pressures and Temperatures

	rate constant [10^{-3} s^{-1}]			
	temperature [K]			
press. [GPa]	525	535	545	555
8.0	1.4 ± 0.1	3.3 ± 0.4	6.4 ± 0.6	–
9.6	0.75 ± 0.02	1.6 ± 0.1	3.2 ± 0.2	7.9 ± 1.3
11.2	–	0.66 ± 0.02	1.4 ± 0.04	2.9 ± 0.4

3.2. Activation Energies and Volumes of Decomposition. Having obtained global decomposition rates at various pressures and temperatures, we determined the activation energies (E_a) and volumes (ΔV^*) for γ-RDX decomposition. These quantities are often used to help characterize transition states and to elucidate decomposition mechanisms in the gas and liquid phases.[21−23] In particular, pressure effects on the activation volume (the difference in partial molar volumes of transition state and reactants) have been utilized to distinguish between different initial steps of decomposition in the liquid phase of HE materials.[21,22] For solid state reactions, complexity arises due to multiple steps, and the E_a and ΔV^* values are weighted means of the processes involved in the reaction mechanism. Therefore, E_a and ΔV^* cannot be assumed to represent a specific reaction. Instead, they represent an overall process dominated by nucleation and growth of the reaction sites in the crystal. To obtain the E_a and ΔV^* values for the γ-RDX, we used the following relations:

$$k = A \exp(-E_a/RT) \quad (2)$$

$$\Delta V^* = -RT(\partial \ln k/\partial P)_T \quad (3)$$

where A is a preexponential factor and R is the gas constant. In Figures 6 and 7, we present plots of ln k values as functions of the inverse of temperature and the pressure, respectively.

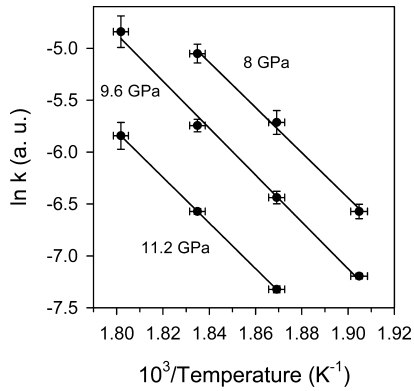

Figure 6. Arrhenius plots of decomposition rates for γ-RDX at three different pressures. Solid lines are from the least-squares fits, and their slopes are proportional to the activation energies. The error bars represent the accuracy for determination of rates and temperature.

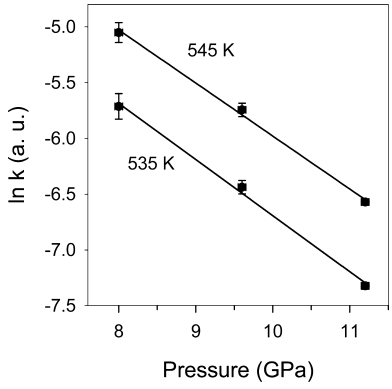

Figure 7. Pressure dependence of decomposition rates for γ-RDX at two different temperatures. Solid lines are from the least-squares fits, and their slopes are proportional to the activation volumes. The error bars represent the accuracy for determination of rates and pressure.

As can be seen in Figure 6, the data show typical Arrhenius dependence for three different pressures, thus permitting a determination of activation energies. The values obtained are 181 ± 10, 188 ± 9, and 183 ± 2 kJ/mol, respectively for 8, 9.6, and 11.2 GPa. Within the experimental error, they seem to be independent of pressure and yield an average value of 184 kJ/mol. This value is somewhat lower than those reported for other RDX phases, which were 207−218 and ∼214 kJ/mol,

dx.doi.org/10.1021/jp307373v | J. Phys. Chem. A 2012, 116, 9680−9688

respectively, at ambient pressure[23] and 1.8 GPa[3] for α-RDX, and ~202 kJ/mol at 3.4 GPa for ε-RDX.[11] Thus, it appears that the activation energy decreases somewhat (~15%) over the 12 GPa pressure range. This small pressure effect on the activation energy is in contrast to large changes in the decomposition rates, indicating the larger pressure induced changes in the preexponential factor. Furthermore, this result differs from the decomposition of RDX in a liquid solution, where a strong pressure effect from 0 to 1.2 GPa was observed on the activation energies.[21]

Figure 7 presents plots of ln k as a function of pressure for two temperatures: 535 and 545 K. The data are represented with almost parallel straight lines obtained from the least-squares fits. The slope of these lines is equal to $-\Delta V^*/RT$, so the activation volume can be calculated at these temperatures. Values for the two temperatures are 2.22 ± 0.14 cm^3/mol (535 K) and 2.13 ± 0.11 cm^3/mol (545 K); within the experimental error, they are the same. However, these values are very different from those reported for the two other phases of RDX, which are 3.19 cm^3/mol for ε-RDX[11] and −5.6 cm^3/mol for α-RDX.[3] The positive activation volumes for ε-RDX and γ-RDX indicate that the pressure decelerates the decomposition in these two phases, while the negative activation volumes indicate decomposition acceleration in α-RDX. The sign change in the activation volume is seen clearly in Figure 8, where we plotted

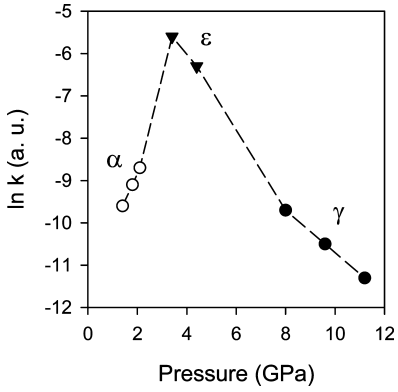

Figure 8. Pressure dependence of decomposition rates for three phases of RDX. All rates correspond to the Arrhenius rate extrapolated to 499 K. The results for the γ-phase are from this work, while those for the ε- and α-phases are from refs 11 and 3, respectively. Dashed lines are guides to the eye.

the global decomposition rates for the three RDX phases as a function of pressure. In Figure 8, the data for α-RDX are from Figure 9 of ref 3 and those for ε-RDX are from our previous work.[11] To make a quantitative comparison between different phases, the rates presented were obtained from an extrapolation to the same temperature of 488 K, assuming their Arrhenius behavior. These data show clear evidence for the change in the global decomposition rate from accelerating to decelerating between ~2 and 3 GPa. Also, we notice that this change takes place in the pressure region, which corresponds to the phase boundary between α-RDX and ε-RDX.[11] However, at this stage it is not clear whether the observed change in the global decomposition rate is associated with the change in the RDX phase. It should be pointed out that a similar pressure trend in the decomposition rate was recently reported for cyclotetramethylene tetranitramine (HMX),[24] another nitramine explosive. In that case, a local maximum in the decomposition rate was observed at ~1−2 GPa.

3.3. Decomposition Products. To gain further insight into the decomposition mechanism of γ-RDX, we made an attempt to determine the decomposition products. Because the decomposed crystal became optically opaque and exhibited large emission background upon laser excitation, Raman measurements were not useful in examining the decomposition species. However, infrared spectra, even from small crystals, provided relatively strong signals from the decomposed samples. To identify decomposition products, the FTIR measurements were performed on the decomposed samples recovered to room temperature. The images of a typical sample, before and after decomposition, used in these measurements are shown in Figure 9. They represent the RDX crystal at

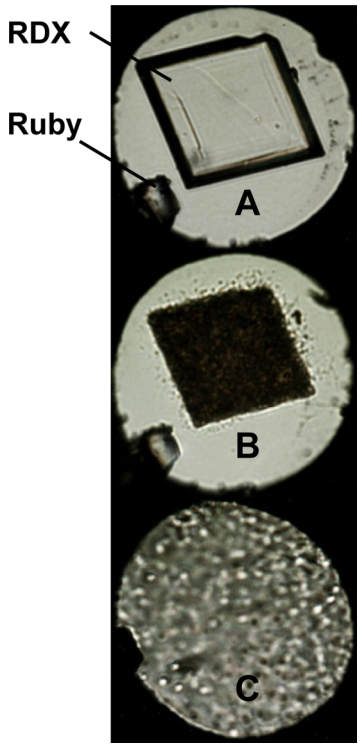

Figure 9. Images of γ-RDX crystal in DAC used in FTIR experiments: (A) before heating at 7 GPa, (B) after decomposition at 7 GPa and then cooled to room temperature, and (C) at ambient conditions upon release of pressure. The diameter of hole in the gasket was ~200 μm.

ambient temperature, under the following conditions: (A) at a pressure of 7 GPa (γ-phase) before decomposition, (B) after decomposition at 7 GPa and ~530 K, and (C) after release of pressure. Images A and B in Figure 9 demonstrate that the sample remained essentially intact after decomposition at high pressure; only a few small particles were seen outside the sample. However, the sample entirely disintegrated upon full release of pressure (Figure 9, image C).

Typical IR spectra of decomposed γ-RDX are shown in Figure 10a. They were acquired on the same decomposed sample at several pressures, upon release of pressure from 7 to 0.7 GPa. Note that the spectra were not obtained from the sample upon full release of pressure because of a lack of the measurable signal, likely due to the escape of gaseous products from the high pressure cell. All spectra were acquired in the

dx.doi.org/10.1021/jp307373v | J. Phys. Chem. A 2012, 116, 9680−9688

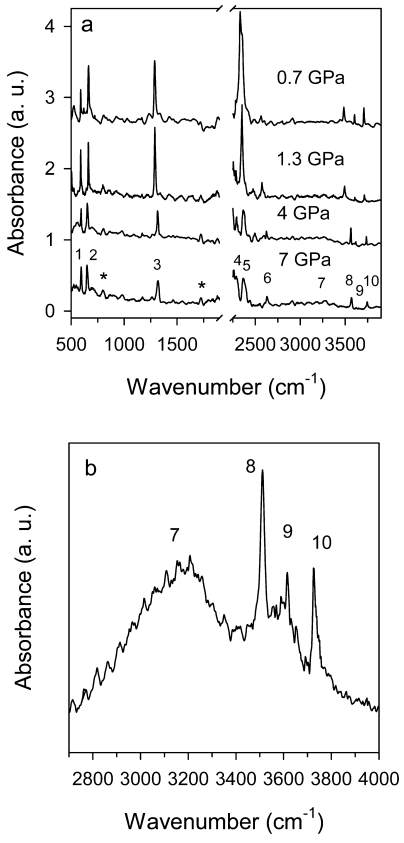

Figure 10. Typical FTIR spectra of decomposed γ-RDX measured at room temperature. (a) Spectra at several pressures during unloading of pressure from 7 to 0.7 GPa. The spectral range from 1900 to 2250 cm^{-1} was removed due to the interference from the absorption of diamond anvils. Numbers from 1 to 10 indicate peaks attributed to the RDX products. The asterisks denote the peaks associated with the background. (b) Part of the IR spectrum to display the pattern of peaks/bands in the high frequency range. This spectrum was obtained from a sample different from the sample used to obtain the spectra shown in panel a. The sample was decomposed at 7 GPa, and the spectrum was measured at 2.6 GPa.

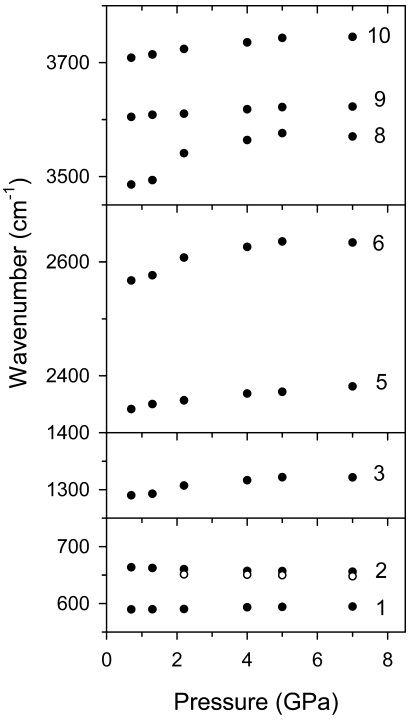

Figure 11. Pressure shifts of vibrational modes of RDX products measured during decrease of pressure from 7.0 to 0.7 GPa. Note that peak 2 is split at high pressure. To distinguish between two peaks, one of the peaks is plotted with open circles. Tentative assignment of the peaks is given in Table 2.

Table 2. IR Vibrational Peaks of γ-RDX Products[a]

	frequency (cm^{-1})		tentative assignment	
peak no.	7 GPa	0.7 GPa	ref[c]	mode
1	595	590	589[d]	N_2O b
2	648, 656[b]	663	657[d]	CO_2 b
3	1322	1290	1293[d]	N_2O s st
4	2287	N/O	2235[d]	N_2O as st
5	2381	2342	2343[d]	CO_2 as st
6	2634	2567		N_2O ot?
7	3200	N/O	3330[e]	OH st
8	3570	3486		N_2O com?
9	3623	3605	3606[f]	CO_2 com
10	3745	3709	3710[f]	CO_2 com

[a]Abbreviations: b, bend; s st, symmetric stretch; as st, asymmetric stretch; ot, overtone; com, combination of modes; N/O, not observed. [b]Doublet at high pressure. [c]Frequencies for various molecules from different references. [d]At 65−80 K in solid matrix, from ref 25. [e]At 15 K, from ref 33. [f]At 2 GPa, from ref 30.

range from 500 to 4000 cm^{-1}. The region from 1900 to 2250 cm^{-1} was removed from the plots because the sample signal overlaps with the strong absorption of diamond anvils. In the frequency range examined, we observed more than 10 peaks/bands that could be attributed to the RDX products. Pressure effects on the positions of peaks were used as one of the criteria to assign their origin. First, we noticed that two low intensity peaks located at ∼802 and ∼1725 cm^{-1}, indicated by asterisks in Figure 10a, do not change position with decreasing pressure. Therefore, they likely originate from the instrument background. The other 10 peaks/bands were attributed to the RDX products and were enumerated from 1 to 10 in Figure 10a. Pressure effects on the frequencies of these peaks are shown in Figure 11, and the frequencies at two pressures, 7 and 0.7 GPa, are listed in Table 2. Figures 10 and 11 show that, upon unloading of pressure, (i) all peaks but one shift to lower frequencies, (ii) only peak 2 (actually, a doublet at high pressure) shifts to higher frequencies, and (iii) there are discontinuities in peak shifts and changes in their intensities, starting below ∼2 GPa. The changes below 2 GPa can be linked to the onset of melting of Ar, used as pressure transmitting medium, as well as to the melting of possible products, e.g., CO_2 and H_2O. In fact, these species melt below 2 GPa, which can significantly affect both the position and intensity of vibrational modes at low pressures.

Peaks 1, 3, and 4 are assigned to N_2O, based on their frequencies[25] and on the previous observation of this molecule in the decomposition of RDX.[3,21,26−29] Specifically, peak 1 is attributed to bending vibrations, while peaks 3 and 4 are attributed to symmetric and asymmetric stretch vibrations, respectively. The last peak is barely seen in our experiments due to the interference from diamond absorption. We believe that peak 6 may also originate from N_2O, as an overtone of the symmetric stretching mode represented by peak 3. Peaks 2, 5, 9, and 10 are assigned to CO_2 based on their frequencies and

dx.doi.org/10.1021/jp307373v | J. Phys. Chem. A 2012, 116, 9680−9688

the pressure dependence,[30−32] as well as on the previous observation of this molecule in the RDX decomposition.[3,21,27,28,30] Peak 2 shows splitting at high pressures and the frequency increase upon decrease of pressure (see Figure 11), which is characteristic of the CO_2 bending mode.[30,31] Furthermore, peak 5 is identified as the CO_2 asymmetric stretching mode, while peaks 9 and 10 are attributed to the combinations of the CO_2 fundamental modes, well established in studies of CO_2.[30]

In Figure 10b, we show the close-up view of the high frequency range to assist in identifying the origin of peaks 7 and 8. It should be noted that this spectrum was obtained on a different sample from that for the spectra presented in Figure 10a. Thus, we can see that the intensity of peak 7 varied somewhat from sample to sample, and this peak was hardly detectable at low pressures. Based on its frequency and broad shape,[31,34] we assigned this peak to the OH stretching mode of water/ice. This product was also observed in previous studies of RDX decomposition.[3,26,27]

In contrast to the peaks mentioned above, we are quite uncertain about the assignment of peak 8. However, based on its frequency, the following origins of this peak can be considered: (1) a combination of fundamental modes of N_2O, (2) the NH stretching mode of the HCN molecules, or (3) the OH stretching mode of H_2O molecules strongly interacting with the surroundings. In all these cases one would expect vibrational frequencies in the range 3400−3500 cm^{-1}, which corresponds to the frequency of peak 8. In particular, the NH vibrations for the HCN molecule were observed around 3450 cm^{-1},[35] the OH vibrations for water molecule hydrogen bonded to organic solvent were observed around 3520 cm^{-1},[36,37] and the combination of N_2O vibrations would produce the peak around 3500 cm^{-1}. To distinguish between these possibilities, it is important to note that peak 8 shows (see Figures 10 and 11) (i) lower intensity than the intensity observed for other fundamental modes in this work, (ii) the largest pressure shift compared to other peaks, and (iii) an initial increase in frequency upon decrease of pressure. We also note that the pressure effects on this peak show some similarity to those observed for peak 6, which was assigned to the N_2O overtone. Given all these observations, it seems that peak 8 could most likely be attributed to the combination of N_2O symmetric (peak 3) and asymmetric stretching (peak 4) modes.

Overall, our FTIR spectra of decomposed γ-RDX indicate the formation of three species, N_2O, CO_2, and H_2O, in the frequency range examined. All these species were previously observed in RDX decomposition at ambient pressure; however, they were often observed along with other products, such as HCN, CH_2O, NO_2, NO, and CO. Because these other species (except NO[29] and CO[38]) have IR active vibrations in the frequency range examined, we could, in principle, expect to observe these vibrations in our spectra. The lack of these vibrations in our data indicates that these species are either produced in very small amounts or are not the final products of the γ-RDX decomposition.

4. DISCUSSION

The main experimental results of this work include the (i) demonstration that pressure decelerates the decomposition of the γ-phase and (ii) identification of final decomposition products as N_2O, CO_2, and H_2O. We discuss these features and compare them to previous studies on RDX at ambient pressure and at elevated pressures to gain insight into the decomposition of the γ-phase.

Thermal decomposition studies of RDX crystals at ambient pressure (α-phase) have established that RDX decomposition has both a heterogeneous and an autocatalytic character.[26] From simultaneous thermogravimetry modulated beam mass spectrometry (STMBMS), hot-stage time-elapsed microscopy, and scanning electron microscopy experiments, it was concluded that the thermal decomposition of RDX (below its melting temperature) may involve reactions that occur in both the gas phase and the bulk.[26] Furthermore, it was proposed that at early times the reactions are mainly controlled by the sublimation of RDX molecules and their decomposition in the gas phase. At later times, reactions are accelerated by the heterogeneous gas phase−solid phase reactions and gas phase reactions of transient species on the surface and in the bulk.

To explain the observed nonmonotonic changes in the global decomposition rates of RDX with pressure (Figure 8), that is, acceleration of rates at low pressures and deceleration above (>2−3 GPa), two scenarios can be considered. The first scenario assumes that mechanisms similar to those at ambient pressure also operate under high pressure, and that the observed maximum in the global decomposition rate around 2−3 GPa is attributed to changes in the competing effects of pressure on different stages of RDX reaction over the entire pressure range.[24] In other words, certain mechanisms can dominate over others at different pressures.

It is well established that pressure can accelerate the gas phase and heterogeneous reactions due to the increase in the collision frequency of gaseous species.[27] Therefore, the acceleration of the global decomposition rate can result from the enhancement of these heterogeneous and autocatalytic reactions. On the other hand, pressure can inhibit sublimation and also hinder the initiation step(s) of decomposition and the formation of some transient species in the reaction. Using the above arguments, as was proposed for HMX,[24] we conjecture the following: At low pressures (<2−3 GPa, α-phase), increasing pressure hinders the initiation step(s) and accelerates the autocatalytic reactions. Though the initiation step(s) are hindered, sufficient amounts of molecules decompose and contribute to accelerating the decomposition. Therefore, the rate of decomposition is determined by the extent of autocatalytic reactions, which increases with pressure. At high pressures (>3 GPa, ε- and γ-phases), the initiation step(s) are significantly hindered, preventing the formation of sufficient amounts of gaseous species for autocatalytic reactions. Thus, the rate of decomposition is controlled by the initiation step(s) and the further rise of pressure decelerates the decomposition. The increasing importance of initiation step(s) with pressure can be seen in Figure 4. As the pressure increases, the contribution of the induction period to the decomposition curves increases significantly.

The second scenario assumes that the observed nonmonotonic change in the global decomposition rate (Figure 8) results from changing the mechanism(s) of decomposition, in particular the initiation step(s). A negative activation volume for the global decomposition below 2−3 GPa could favor the initiation step(s), which involves (involve) elimination reactions rather than the formation of radicals. Above 3 GPa, a positive activation volume suggests the contribution of reactions involving bond cleavage. In the case of RDX, it is generally accepted that the initial steps of decomposition at ambient pressure can involve three parallel channels: the

homolysis of the N−NO_2 bond, elimination of HONO, and the concerted triple scission of C−N bonds. Therefore, the HONO elimination could dominate below 2−3 GPa (α-phase), but the N−NO_2 and C−N bond cleavages could contribute at higher pressures (ε- and γ-phases). The HONO elimination would lead to formation of 1,3,5-triazine, which was not detected by FTIR, likely because it was consumed in subsequent reactions. On the other hand, the cleavage of the N−N and C−N bonds would lead to the presence of N_2O, CO_2, H_2O, NO, and CO in the final decomposition product. The last two species, as mentioned in section 3.3, could not be identified due to the interference from diamond absorption. Therefore, we can neither confirm nor rule out their presence in the decomposed γ-RDX. However, it is worth noting that high pressure studies on α-RDX, both in the solid phase[3] and in solution,[21] mentioned the presence of the same three species in the IR spectra as for the γ-phase.

Since the data on decomposition species in the α- and γ-phases are incomplete, and therefore inconclusive, we cannot definitely distinguish between the two scenarios presented: pressure changes the relative importance between the heterogeneous and autocatalytic reactions and initiation step(s) or pressure changes the initiation step(s) of the mechanism. Despite this indistinguishability, our data on the pressure deceleration of decomposition in γ-RDX indicate that the pressure increase hinders the initiation step(s) related to the cleavage of the N−NO_2 and/or C−N bonds. Because the calculated energy barriers for N−N dissociation are much lower than for the C−N dissociation,[39] we favor the N−NO_2 homolysis over the C−N concerted triple scission. However, more work is required to test this conjecture and to examine the evolution of decomposition intermediates to determine the decomposition pathways leading to the observed species. This could likely be accomplished using time-resolved FTIR measurements.

5. SUMMARY AND CONCLUSIONS

Vibrational spectroscopy and optical imaging measurements in diamond anvil cell experiments were used to examine the γ-phase of RDX crystals at high pressures and high temperatures, and to provide new insight into the reactive behavior of RDX at conditions relevant to shock wave initiation. These studies, performed under static compression from 6 to 12 GPa and at temperatures up to 600 K, provided global decomposition kinetics, energies and volumes of activation, and decomposition products for γ-RDX. In particular, we found that (i) decomposition kinetics are autocatalytic, (ii) rates of global decomposition decrease with pressure but increase with temperature, (iii) activation volumes are positive, (iv) both energies and volumes of activation are apparently not pressure dependent in the $P-T$ range examined, and (v) CO_2, N_2O, and H_2O are the main decomposition products. We also established that pressure effects on the γ-phase decomposition characteristics are similar to those for the ε-phase but opposite those for the α-phase. The pressure-induced deceleration of decomposition in γ-RDX may indicate that the pressure increase hinders the initiation step(s) related to the bond homolysis.

Finally, this work extends and complements our previous studies on the polymorphism, stability, phase diagram, and decomposition of RDX under extreme conditions of pressure and temperatures. It provides insight into decomposition of the γ-phase of RDX, which is found to play a key role in the reactive behavior of RDX under static and dynamic compression.

AUTHOR INFORMATION

Corresponding Author

*E-mail: dreger@wsu.edu.

Notes

The authors declare no competing financial interest.

ACKNOWLEDGMENTS

Dr. D. E. Hooks from Los Alamos National Laboratory is thanked for providing the RDX crystals. This work was supported by NNSA-DOE Grant DE-NA0000970 and ONR-MURI Grant N00014-06-1-0459.

REFERENCES

(1) Choi, C. S.; Prince, E. *Acta Crystallogr., Sect. B* **1972**, *28*, 2857−2862.
(2) Baer, B. J.; Oxley, J.; Nicol, M. *High Pressure Res.* **1990**, *2*, 99−108.
(3) Miller, P. J.; Block, S.; Piermarini, G. J. *Combust. Flame* **1991**, *83*, 174−184.
(4) Dreger, Z. A.; Gupta, Y. M. *J. Phys. Chem. B* **2007**, *111*, 3893−3903.
(5) Ciezak, J. A.; Jenkins, T. A.; Liu, Z.; Hemley, R. J. *J. Phys. Chem. A* **2007**, *111*, 59−63.
(6) Davidson, A. J.; Oswald, I. D. H.; Francis, D. J.; Lennie, A. R.; Marshall, W. G.; Millar, D. I. A.; Pulham, C. R.; Warren, J. E.; Cumming, A. S. *Cryst. Eng. Commun.* **2008**, *10*, 162−165.
(7) Karpowicz, R. J.; Sergio, S. T.; Brill, T. B. *Ind. Eng. Chem. Prod. Res. Dev.* **1983**, *22*, 363−365.
(8) Torres, P.; Mercado, L.; Cotte, I.; Hernandez, S. P.; Mina, N.; Santana, A.; Chamberlain, R. T.; Lareau, R.; Castro, M. E. *J. Phys. Chem. B* **2004**, *108*, 8799−8805.
(9) Millar, D. I.; Oswald, I. D. H.; Francis, D. J.; Marshall, W. G.; Pulham, C. R.; Warren, J. E.; Cumming, A. S. *Chem. Commun.* **2009**, *5*, 562−564.
(10) Ciezak, J. A.; Jenkins, T. A. *Propellants, Explos., Pyrotech.* **2008**, *33*, 390−395.
(11) Dreger, Z. A.; Gupta, Y. M. *J. Phys. Chem. A* **2010**, *114*, 8099−8105.
(12) Dreger, Z. A.; Gupta, Y. M. *J. Phys. Chem. A* **2010**, *114*, 7038−7047.
(13) Millar, D. I.; Oswald, I. D. H.; Barry, C.; Francis., D. J.; Marshall, W. G.; Pulham, C. R.; Cumming, A. S. *Chem. Commun.* **2010**, *46*, 5662−5664.
(14) Patterson, J. E.; Dreger, Z. A.; Gupta, Y. M. *J. Phys. Chem. B* **2007**, *111*, 10897−10904.
(15) Patterson, J. E.; Dreger, Z. A.; Miao, M. S.; Gupta, Y. M. *J. Phys. Chem. A* **2008**, *112*, 7374−7382.
(16) Dreger, Z. A.; Gupta, Y. M. *J. Phys. Chem. A* **2012**, *116*, 8713−8717.
(17) Sun, B.; Dreger, Z. A.; Gupta, Y. M. *J. Phys. Chem. A* **2008**, *112*, 10546−10551.
(18) Brown, W. E.; Dollimore, D.; Galwey, A. In *Reactions in the Solid State, Comprehensive Chemical Kinetics*; Bamford, C. H., Tipper, C. F. H., Eds.; Elsevier: Amsterdam, 1980.
(19) Sometimes the Prout−Tompkins (PT) model is used in the multiparameter form, which is called the extended PT (e-PT) model. However, it includes a number of variables associated with the reaction order. The selection of these variables is somewhat arbitrary and often leads to ambiguity in deriving the reliable decomposition rates.
(20) Piermarini, G. J.; Block, S.; Miller, P. J. *J. Phys. Chem.* **1987**, *91*, 3872−3878; **1989**, *93*, 457−462.
(21) Wang, J.; Brower, K. R.; Naud, D. L. *J. Org. Chem.* **1997**, *62*, 9055−9060.
(22) Naud, D. L.; Brower, K. R. *J. Org. Chem.* **1992**, *57*, 3303−3308.

(23) Brill, T. B.; Gongwer, P. E.; Williams, G. K. *J. Phys. Chem.* **1994**, *98*, 12242−12247.
(24) Glascoe, E. A.; Zaug, J. M.; Burnham, A. K. *J. Phys. Chem. A* **2009**, *113*, 13548−13555.
(25) Yamada, H.; Person, W. B. *J. Chem. Phys.* **1964**, *41*, 2478−2487.
(26) Maharrey, S.; Behrens, R. *J. Phys. Chem. A* **2005**, *109*, 11236−11249.
(27) Brill, T. B.; Brush, P. J. *Philos. Trans. R. Soc. London, A* **1992**, *339*, 377−385.
(28) Botcher, T. R; Wight, C. A. *J. Phys. Chem.* **1993**, *97*, 9149−9153.
(29) Choi, M.; Kim, H.; Chung, C. *J. Phys. Chem.* **1995**, *99*, 15785−15789.
(30) Lu, R.; Hofmeister, A. M. *Phys. Rev. B* **1995**, *52*, 3985−3992.
(31) McCluskey, M. D.; Zhuravlev, K. K. *J. Chem. Phys.* **2002**, *116*, 1607−1612.
(32) Castano, J. A. G.; Fantoni, A.; Romano, R. M. *J. Mol. Struct.* **2008**, *881*, 68−75.
(33) Bernstein, M. P.; Cruikshank, D. P.; Sandford, S. A. *ICARUS* **2005**, *179*, 527−534.
(34) Ceppatelli, M.; Bini, R.; Schettino, V. *Proc. Natl. Acad. Sci. U.S.A.* **2009**, *106*, 11454−11459.
(35) Suzuki, I.; Pariseau, M. A.; Overend, J. *J. Chem. Phys.* **1966**, *44*, 3561−3567.
(36) Gilijamse, J. J.; Lock, A. J.; Bakker, H. J. *Proc. Natl. Acad. Sci. U.S.A.* **2005**, *102*, 3202−3207.
(37) Tummala, N. R.; Striolo, A. *J. Phys. Chem. B* **2008**, *112*, 10675−10683.
(38) The CO stretching vibration is expected around 2070 cm^{-1}; this value is in the spectral range that is not measured in our experiments due to the strong diamond absorption.
(39) Miao, M. S.; Dreger, Z. A.; Patterson, J. E.; Gupta, Y. M. *J. Phys. Chem. A* **2008**, *112*, 7383−7390.